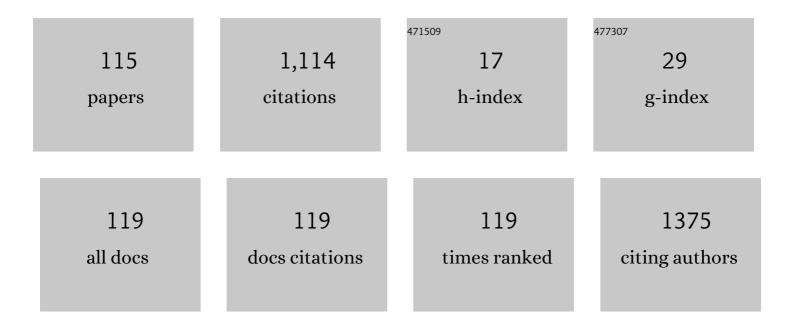
Raynald Gauvin

List of Publications by Year in descending order

Source: https://exaly.com/author-pdf/9915035/publications.pdf Version: 2024-02-01



#	Article	IF	CITATIONS
1	Silicon doped carbon nanotubes as high energy anode for lithium-ion batteries. Materials Today Communications, 2022, 30, 103158.	1.9	8
2	Tetragonal reconstruction and monoclinic variants rearrangement during heat treatment in zirconia. Journal of the American Ceramic Society, 2022, 105, 5436-5447.	3.8	3
3	Phase differentiation based on x-ray energy spectrum correlation with an energy dispersive spectrometer (EDS). Ultramicroscopy, 2022, 238, 113534.	1.9	2
4	Structural Study of Sulfur-Added Carbon Nanohorns. Materials, 2022, 15, 3412.	2.9	1
5	Extraction of 3D quantitative maps using EDS-STEM tomography and HAADF-EDS bimodal tomography. Ultramicroscopy, 2021, 220, 113166.	1.9	Ο
6	Plasmon-Enhanced Hydrogenation of 1-Dodecene and Toluene Using Ruthenium-Coated Gold Nanoparticles. ACS Applied Nano Materials, 2021, 4, 1596-1603.	5.0	6
7	Scanning Electron Microscopy versus Transmission Electron Microscopy for Material Characterization: A Comparative Study on High-Strength Steels. Scanning, 2021, 2021, 1-19.	1.5	13
8	High-Resolution Electron Microscopy Analysis of Malaria Hemozoin Crystals Reveals New Aspects of Crystal Growth and Elemental Composition. Crystal Growth and Design, 2021, 21, 5521-5533.	3.0	5
9	Enhancing Singlet Oxygen Photocatalysis with Plasmonic Nanoparticles. ACS Applied Materials & Interfaces, 2021, 13, 35606-35616.	8.0	22
10	The f-ratio model for quantitative X-ray microanalysis. Talanta, 2021, 235, 122765.	5.5	5
11	Study of the Peak to Background (P/B) Method Behavior as a Function of Take-Off Angle, Tilt Angle, Particle Size, and Beam Energy. Scanning, 2021, 2021, 1-7.	1.5	1
12	In Situ and In Operando Techniques to Study Li-Ion and Solid-State Batteries: Micro to Atomic Level. Inorganics, 2021, 9, 85.	2.7	5
13	Improvement of the energy resolution of energy dispersive spectrometers (EDS) using Richardson–Lucy deconvolution. Ultramicroscopy, 2020, 209, 112886.	1.9	7
14	Investigation of the Effect of Magnification, Accelerating Voltage, and Working Distance on the 3D Digital Reconstruction Techniques. Scanning, 2020, 2020, 1-9.	1.5	1
15	Core hole screened electron energy loss calculations of beam damaged lithium fluoride. Ultramicroscopy, 2020, 219, 113126.	1.9	Ο
16	Direct observation of lithium metal dendrites with ceramic solid electrolyte. Scientific Reports, 2020, 10, 18410.	3.3	45
17	The Impact of Chemical Bonding on Mass Absorption Coefficients of Soft X-rays. Microscopy and Microanalysis, 2020, 26, 741-749.	0.4	2
18	Secondary Fluorescence of 3D Heterogeneous Materials Using a Hybrid Model. Microscopy and Microanalysis, 2020, 26, 484-496.	0.4	2

#	Article	IF	CITATIONS
19	A hydrodynamic approach to electron beam imaging using a Bloch wave representation. Ultramicroscopy, 2020, 212, 112979.	1.9	1
20	Multivariate Statistical Analysis on a SEM/EDS Phase Map of Rare Earth Minerals. Scanning, 2020, 2020, 1-11.	1.5	7
21	Inverse modeling for quantitative X-ray microanalysis applied to 2D heterogeneous materials. Ultramicroscopy, 2020, 219, 113117.	1.9	2
22	Microstructure evolution of Inconel 738 fabricated by pulsed laser powder bed fusion. Progress in Additive Manufacturing, 2019, 4, 97-107.	4.8	30
23	Using Deep Learning to Deconvolute Complex Spectra for Hyperspectral Imaging Applications. Microscopy and Microanalysis, 2019, 25, 178-179.	0.4	Ο
24	EELS Monitoring of Beam-Induced Dynamic Transformation of Lithium Materials at 30 keV. Microscopy and Microanalysis, 2019, 25, 2168-2169.	0.4	0
25	Extending Monte Carlo Simulations of Electron Microscopy Images and Hyperspectral Images in a User-Friendly Framework. Microscopy and Microanalysis, 2019, 25, 222-223.	0.4	2
26	The Impact of Phase on Mass Absorption Coefficients Using Soft X-ray Emission Spectrometry. Microscopy and Microanalysis, 2019, 25, 250-251.	0.4	0
27	Wave-packet numerical investigation of thermal diffuse scattering: A time-dependent quantum approach to electron diffraction simulations. Micron, 2019, 126, 102737.	2.2	1
28	<i>In-Situ</i> Characterization of Lithium Native Passivation Layer in A High Vacuum Scanning Electron Microscope. Microscopy and Microanalysis, 2019, 25, 866-873.	0.4	5
29	The f-ratio quantification method applied to standard minerals with a cold field emission SEM/EDS. Talanta, 2019, 204, 213-223.	5.5	3
30	Secondary Fluorescence Correction for Characteristic and Bremsstrahlung X-Rays Using Monte Carlo X-ray Depth Distributions Applied to Bulk and Multilayer Materials. Microscopy and Microanalysis, 2019, 25, 92-104.	0.4	8
31	The <i>f</i> -Ratio Quantification Method for X-ray Microanalysis Applied to Mg–Al–Zn Alloys. Microscopy and Microanalysis, 2019, 25, 58-69.	0.4	4
32	In situ observation of solid electrolyte interphase evolution in a lithium metal battery. Communications Chemistry, 2019, 2, .	4.5	52
33	Electron energy-loss spectroscopy (EELS) with a cold-field emission scanning electron microscope at low accelerating voltage in transmission mode. Ultramicroscopy, 2019, 203, 21-36.	1.9	17
34	Microstructure and mechanical property connections for a punched non-oriented electrical steel lamination. Materials Science & Engineering A: Structural Materials: Properties, Microstructure and Processing, 2018, 725, 456-465.	5.6	15
35	Secondary Fluorescence Correction of 3D Heterogeneous Materials for Quantitative X-ray Microanalysis. Microscopy and Microanalysis, 2018, 24, 778-779.	0.4	0
36	Low Voltage Analytical Possibilities in a Scanning Electron Microscope in Transmission Mode at 30 kV: EDS, EELS and CBED at the Nanoscale. Microscopy and Microanalysis, 2018, 24, 2036-2037.	0.4	0

#	Article	IF	CITATIONS
37	The Joy of Nanoscale Imaging and Spectroscopy in a Low Accelerating Voltage Scanning Transmitted Electron Microscope. Microscopy and Microanalysis, 2018, 24, 640-641.	0.4	0
38	In Situ Scanning Electron Microscopy Detection of Carbide Nature of Dendrites in Li–Polymer Batteries. Nano Letters, 2018, 18, 7583-7589.	9.1	86
39	Nanoscale Lithium Quantification in LiXNiyCowMnZO2 as Cathode for Rechargeable Batteries. Scientific Reports, 2018, 8, 17575.	3.3	32
40	Monte Carlo Simulation of Surface Semi-Spherical Inclusions Using MC X-ray. Microscopy and Microanalysis, 2018, 24, 740-741.	0.4	0
41	EELS Analysis of Bulk Plasmon Harmonics of Aluminium at 30 keV. Microscopy and Microanalysis, 2018, 24, 464-465.	0.4	3
42	The Standard-based f-ratio Quantitative X-Ray Microanalysis Method for a Field Emission SEM. Microscopy and Microanalysis, 2018, 24, 732-733.	0.4	1
43	Influence of Substrate Characteristics on Single Ti Splat Bonding to Ceramic Substrates by Cold Spray. Journal of Thermal Spray Technology, 2018, 27, 1011-1024.	3.1	12
44	Fabrication of Crack-Free Nickel-Based Superalloy Considered Non-Weldable during Laser Powder Bed Fusion. Materials, 2018, 11, 1288.	2.9	47
45	Hollow silica capsules for amphiphilic transport and sustained delivery of antibiotic and anticancer drugs. RSC Advances, 2018, 8, 24883-24892.	3.6	14
46	My Joy of Research in SEM. Microscopy and Microanalysis, 2018, 24, 602-603.	0.4	1
47	In Situ TEM Investigation of Electron Irradiation Induced Metastable States in Lithium-Ion Battery Cathodes: Li ₂ FeSiO ₄ versus LiFePO ₄ . ACS Applied Energy Materials, 2018, 1, 3180-3189.	5.1	20
48	Use of an Annular Silicon Drift Detector (SDD) Versus a Conventional SDD Makes Phase Mapping a Practical Solution for Rare Earth Mineral Characterization. Microscopy and Microanalysis, 2018, 24, 238-248.	0.4	8
49	The qualitative fâ€ratio method applied to electron channellingâ€induced xâ€ray imaging with an annular silicon drift detector in a scanning electron microscope in the transmission mode. Journal of Microscopy, 2017, 267, 288-298.	1.8	3
50	Growth modes for monoclinic yttriaâ€stabilized zirconia during the martensitic transformation. Journal of the American Ceramic Society, 2017, 100, 4874-4883.	3.8	13
51	Quantification of Thin Specimens in a Scanning Transmission Electron Microscope at Low Accelerating Voltage using the f-ratio Method. Microscopy and Microanalysis, 2017, 23, 236-237.	0.4	1
52	The Effect of Submicron Second-Phase Particles on the Rate of Grain Refinement in a Copper-Oxygen Alloy During Cold Spray. Journal of Thermal Spray Technology, 2017, 26, 1509-1516.	3.1	18
53	Mapping Data with Heavily Overlapped Spectral Features. Microscopy and Microanalysis, 2017, 23, 216-217.	0.4	0
54	Open Source Software for Quantitative X-ray Microanalysis: openMicroanalysis. Microscopy and Microanalysis, 2017, 23, 234-235.	0.4	0

#	Article	IF	CITATIONS
55	The Fluorescence Correction of Multilayer Materials for Quantitative X-ray Microanalysis. Microscopy and Microanalysis, 2017, 23, 218-219.	0.4	1
56	Low Accelerating Voltage Scanning Transmitted Electron Microscope: Imaging, Diffraction, X-ray Microanalysis, and Electron Energy-Loss Spectroscopy at the Nanoscale. Microscopy and Microanalysis, 2017, 23, 528-529.	0.4	2
57	The f-ratio Quantification Method for X-ray Microanalysis with a Field Emission SEM Applied to Multi-Elements Specimen. Microscopy and Microanalysis, 2017, 23, 1046-1047.	0.4	4
58	Thermal Stability of Cryomilled Al-Mg-Er Powders. Journal of Nanomaterials, 2017, 2017, 1-17.	2.7	2
59	High Spatial Resolution Spectroscopy in a FE-SEM: X-ray Microanalysis and Electron Energy-Loss Spectroscopy. Microscopy and Microanalysis, 2017, 23, 1044-1045.	0.4	2
60	About the contrast of δ' precipitates in bulk Al–Cu–Li alloys in reflection mode with a fieldâ€emission scanning electron microscope at low accelerating voltage. Journal of Microscopy, 2017, 268, 107-118.	1.8	7
61	X-ray Emission From Thin Films on a Substrate - Experiments and Simulation. Microscopy and Microanalysis, 2016, 22, 400-401.	0.4	4
62	Determination of Soft X-ray Emission Spectroscopy Parameters using Experimental Data for Quantitative Microanalysis. Microscopy and Microanalysis, 2016, 22, 408-409.	0.4	4
63	Deformation Analysis of Forsterite Olivine Using Electron Channeling Contrast Imaging and Electron Backscatter Diffraction. Microscopy and Microanalysis, 2016, 22, 1792-1793.	0.4	2
64	Can we detect Li K Xâ€ray in lithium compounds using energy dispersive spectroscopy?. Scanning, 2016, 38, 571-578.	1.5	77
65	X-ray Microanalysis Phase Map on Rare Earth Minerals with a Conventional and an Annular Silicon Drift Detector. Microscopy and Microanalysis, 2016, 22, 96-97.	0.4	1
66	Monte Carlo Simulations of Electron Energy-Loss Spectra with the Addition of Fine Structure from Density Functional Theory Calculations. Microscopy and Microanalysis, 2016, 22, 219-229.	0.4	1
67	On Rotation Contour Contrast in Hot-Compressed Magnesium Alloys in a Scanning Electron Microscope. Metallography, Microstructure, and Analysis, 2016, 5, 188-195.	1.0	1
68	A universal equation for computing the beam broadening of incident electrons in thin films. Ultramicroscopy, 2016, 167, 21-30.	1.9	16
69	Dark-Field Imaging based on Post-Processing of Electron Backscatter Diffraction Patterns in a Scanning Electron Microscope. Microscopy and Microanalysis, 2015, 21, 2031-2032.	0.4	1
70	Characterization of Hot-Compressed Magnesium Alloys in a Scanning Electron Microscope. Microscopy and Microanalysis, 2015, 21, 599-600.	0.4	0
71	Rotation Axes Analysis of Deformed Magnesium Using Electron Backscatter Diffraction and Rotation Contour Contrast Reconstruction. Microscopy and Microanalysis, 2015, 21, 2379-2380.	0.4	0
72	Origins and Contrast of the Electron Signals at Low Accelerating Voltage and with Energy-Filtering in the FE-SEM for High Resolution Imaging. Microscopy and Microanalysis, 2015, 21, 705-706.	0.4	2

#	Article	IF	CITATIONS
73	Characterization of Advanced Nanomaterials for Lithium Ion Batteries Cathodes. Microscopy and Microanalysis, 2015, 21, 677-678.	0.4	1
74	High Spatial Resolution Quantification X-ray Microanalysis in a Field Emission Scanning Electron Microscope with an Annular Silicon Drift Detector. Microscopy and Microanalysis, 2015, 21, 2359-2360.	0.4	1
75	Rotation axes analysis of deformed magnesium based on rotation contour contrast in a scanning electron microscope. Ultramicroscopy, 2015, 154, 42-48.	1.9	6
76	Microstructure and Mechanical Properties of Ti Cold-Spray Splats Determined by Electron Channeling Contrast Imaging and Nanoindentation Mapping. Microscopy and Microanalysis, 2015, 21, 570-581.	0.4	38
77	Dark-field imaging based on post-processed electron backscatter diffraction patterns of bulk crystalline materials in a scanning electron microscope. Ultramicroscopy, 2015, 148, 123-131.	1.9	14
78	High Resolution Imaging in the Field Emission Scanning Electron Microscope at Low Accelerating Voltage and with Energy-Filtration of the Electron Signals. Microscopy and Microanalysis, 2014, 20, 16-17.	0.4	0
79	Spatial Distribution of Light Scattering and Absorption Interactions with TiO2- Nanoparticles from Monte Carlo and Generalized-Multiparticle-Mie based Simulations for Dye-Sensitized Solar Cell Analysis and Optimization. Microscopy and Microanalysis, 2014, 20, 548-549.	0.4	Ο
80	Microstructure Refinement of Cold-Sprayed Copper Investigated By Electron Channeling Contrast Imaging. Microscopy and Microanalysis, 2014, 20, 1499-1506.	0.4	22
81	X-Ray Microanalysis with High Spatial Resolution and High Counts Rate with a State of the Art Field Emission Scanning Electron Microscope. Microscopy and Microanalysis, 2014, 20, 650-651.	0.4	1
82	Microstructural Characterization of Mg–0.3Al–0.2Ca Alloy Using Ion Milling Surface Preparation Technique. Metallography, Microstructure, and Analysis, 2014, 3, 257-262.	1.0	3
83	Magnetic domain structure and crystallographic orientation of electrical steels revealed by a forescatter detector and electron backscatter diffraction. Ultramicroscopy, 2014, 142, 40-49.	1.9	25
84	lonic Liquid Used for Charge Compensation for High-Resolution Imaging and Analysis in the FE-SEM. Microscopy and Microanalysis, 2014, 20, 38-39.	0.4	5
85	Transmission Electron Forward Scattered Diffraction and Low Voltage SEM/STEM Characterization of Binder-Free TiO2 Electrodes. Microscopy and Microanalysis, 2014, 20, 492-493.	0.4	1
86	X-ray Quantitative Microanalysis Maps across Interfaces of a Cu-Al Roll Bonded Laminate with an Annular Silicon Drift Detector. Microscopy and Microanalysis, 2014, 20, 676-677.	0.4	1
87	Electron Channeling Contrast Observations in Deformed Magnesium Alloys. Microscopy and Microanalysis, 2014, 20, 1452-1453.	0.4	1
88	Magnetic Domain Structure and Crystal Orientation Revealed by a Forescatter Detector and Electron Backscatter Diffraction Microscopy and Microanalysis, 2014, 20, 1458-1459.	0.4	0
89	Sliding-induced Microstructure of Cold-Sprayed Copper Coating Observed by Electron Channeling Contrast Imaging. Microscopy and Microanalysis, 2014, 20, 2104-2105.	0.4	3
90	Evaluation of strain rate sensitivity by constant load nanoindentation. Journal of Materials Science, 2012, 47, 7189-7200.	3.7	51

#	Article	IF	CITATIONS
91	What Remains to Be Done to Allow Quantitative X-Ray Microanalysis Performed with EDS to Become a True Characterization Technique?. Microscopy and Microanalysis, 2012, 18, 915-940.	0.4	26
92	Consolidation of Al2O3/Al Nanocomposite Powder by Cold Spray. Journal of Thermal Spray Technology, 2011, 20, 275-284.	3.1	31
93	Nanocrystalline TiO2 thin film electrodes for dye-sensitized solar cell applications. Jom, 2009, 61, 52-57.	1.9	18
94	Thermal stability of SrFeO3/Al2O3 thin films: Transmission electron microscopy study and conductometric sensing response. Journal of Applied Physics, 2008, 104, .	2.5	13
95	A Universal Equation for the Emission Range of X Rays from Bulk Specimens. Microscopy and Microanalysis, 2007, 13, 354-357.	0.4	8
96	Transmission electron microscopy investigation of interfacial reactions between SrFeO3 thin films and silicon substrates. Journal of Materials Research, 2007, 22, 76-88.	2.6	0
97	Quantitative X-Ray Microanalysis of Heterogeneous Materials Using Monte Carlo Simulations. Mikrochimica Acta, 2006, 155, 75-81.	5.0	12
98	Win X-ray: A New Monte Carlo Program that Computes X-ray Spectra Obtained with a Scanning Electron Microscope. Microscopy and Microanalysis, 2006, 12, 49-64.	0.4	87
99	X-ray microanalysis of real materials using Monte Carlo simulations. Surface and Interface Analysis, 2005, 37, 875-886.	1.8	19
100	Introduction: Characterization of Nonconductive Materials. Microscopy and Microanalysis, 2004, 10, 669-669.	0.4	0
101	X-Ray Microanalysis of Real Materials Using Monte Carlo Simulations. Mikrochimica Acta, 2004, 145, 41-47.	5.0	7
102	Possibility of charge contrast imaging of polymeric materials. Scanning, 2003, 25, 240-242.	1.5	5
103	Contrast of Multilayed Structures in a Field Emission Gun Scanning Electron Microscope. Microscopy and Microanalysis, 2003, 9, 988-989.	0.4	Ο
104	On the Contrast and Resolution of Secondary and Backscattered Electron Images in a FE-SEM. Microscopy and Microanalysis, 2003, 9, 970-971.	0.4	2
105	Spatial Resolution Limits for X-ray Microanalysis of Bulk Samples. Microscopy and Microanalysis, 2003, 9, 536-537.	0.4	1
106	Win X-ray, The Monte Carlo Program for X-ray Microanalysis in the Scanning Electron Microscope. Microscopy and Microanalysis, 2003, 9, 32-33.	0.4	7
107	On the Simulation of True EDS X-Ray Spectra. Microscopy and Microanalysis, 2002, 8, 430-431.	0.4	0
108	Physics of Low Voltage Scanning Electron Microscopy. Microscopy and Microanalysis, 2002, 8, 116-117.	0.4	13

#	Article	IF	CITATIONS
109	X-Ray Microanalysis of a Coated Non-Conductive Specimen: Monte Carlo Simulation. Microscopy and Microanalysis, 2002, 8, 1462-1463.	0.4	0
110	SEM-EDS Quantitative Analysis of Aerosols ≥ 80nm: Impacts on Atmospheric Aerosol Characterization Campaigns. Microscopy and Microanalysis, 2002, 8, 1482-1483.	0.4	3
111	Evaluation of Current Standardless Quantitative Analysis Programs using Energy Dispersive Spectrometry in the SEM. Microscopy and Microanalysis, 2002, 8, 1470-1471.	0.4	0
112	Quantitative X-Ray Microanalysis with a Low Voltage Scanning Electron Microscope. Microscopy and Microanalysis, 2002, 8, 1474-1475.	0.4	0
113	Modeling Contrasts in Variable Pressure Scanning Electron Microscopes. Microscopy and Microanalysis, 2002, 8, 452-453.	0.4	0
114	WinX-Ray: A New Monte Carlo Program for the Simulation of X-Ray and Charging Materials. Microscopy and Microanalysis, 2002, 8, 1498-1499.	0.4	10
115	A method to measure the effective gas path length in the environmental or variable pressure scanning electron microscope. Scanning, 2002, 24, 171-174.	1.5	8